

PAPER

Application of a type of strain block FBG sensor for strain measurements of squeezing rock in a deep-buried tunnel


To cite this article: Guojun Wu *et al* 2017 *Meas. Sci. Technol.* **28** 115001

View the [article online](#) for updates and enhancements.

Related content

- [Wavelength hopping due to spectral distortion in dynamic FBG sensor measurements](#)
S Webb, K Peters, M Zikry et al.
- [Optical fiber sensors for spacecraft applications](#)
E J Friebele, C G Askins, A B Bosse et al.
- [Investigation of the strain transfer for surface-attached optical fiber strain sensors](#)
Kai Tai Wan, Christopher K Y Leung and Noah G Olson

Application of a type of strain block FBG sensor for strain measurements of squeezing rock in a deep-buried tunnel

Guojun Wu¹ , Weizhong Chen^{1,2}, Yonghao Dai¹, Jianping Yang¹, Xianjun Tan¹ and Hongming Tian¹

¹ State Key Laboratory of Geomechanics and Geotechnical Engineering, Institute of Rock and Soil Mechanics, Chinese Academy of Sciences, Wuhan 430071, People's Republic of China

² Research Center of Geotechnical & Structural Engineering, Shandong University, Jinan 250061, People's Republic of China

E-mail: gjuw@whrsm.ac.cn

Received 26 April 2017, revised 19 July 2017

Accepted for publication 1 August 2017

Published 5 October 2017



CrossMark

Abstract

Tunneling in squeezing rock often encounters large deformation, which threatens the safety and stability of tunnel support during tunnel construction. In this work, to acquire a greater amount of strain sensor data to fully understand the stress/strain state of surrounding rock during tunnel excavation, a special type of strain block with fiber Bragg grating (FBG) sensors has been introduced, which is characterized by three groups of FBG strain rosettes adhered to three adjacent surfaces of the block, respectively, and each strain rosette distributed in the form of a 0°–45°–90° arrangement. Applying this type of FBG strain block sensor to a deep-buried tunnel in squeezing rock, six strain components in one strain block (representative of strain state of a point in rock) could be obtained with the processing method. The monitoring results can reflect the effect of tunnel excavation due to abrupt changes of strain monitored in rock, and were verified as being in reasonable agreement with numerical simulation. Therefore, the strain block with FBG sensors can be applicable in measuring strains in squeezing rock.

Keywords: FBG, strain, monitoring, soft rock, tunnel

(Some figures may appear in colour only in the online journal)

1. Introduction

Tunneling in squeezing rock often encounters large deformation and cave-ins of soft rock as well as support failure during tunnel construction. In order to avoid support failure or instability when tunneling, the strain/stress distribution in rock mass during the process of tunnel excavation are fundamental to be understood [1–3]. Although many related studies have been carried out in this area by all kinds of research methods, construction measurement is undoubtedly a direct means to understanding the conditions of surrounding rock and support, which provides first-hand information regarding the stability and safety of engineering construction [4–6].

For *in situ* measurements, a fiber Bragg grating (FBG) sensor, based on a type of digital optical sensor technology,

has been developed in recent years for its long-term stability and high precision measurement. It is often used in monitoring the stress/strain and displacement state of objectives as well as temperature distributed measurements in case of fire [7, 8]. For the application of FBG sensors in strain measurement, a number of innovations in measuring methods and the fabrication of sensors have been achieved. Gill *et al* [9] presented a genetic algorithm for the interrogation of optical FBG strain sensors. Ma *et al* [10] demonstrated a simple and fast interrogation method for the dynamic and/or static strain gauge using a reflection spectrum from two superimposed FBGs. Schizas *et al* [11] proposed a method for nonhomogeneous strain monitoring of composite structures with embedded wavelength multiplexed FBG sensors. Feng *et al* [12] reported the investigation of the Brillouin optical time-domain reflectometer for assessing

damage in structural members. Peters *et al* [13] investigated the use of embedded optical FBGs to measure non-uniform strain field near a stress concentration within a solid structure. Rodriguez-Cobo *et al* [14], Zhou *et al* [15] and Liu *et al* [16] designed and developed different optical fiber strain sensors for composite structures. Gangopadhyay *et al* [17] and Torres *et al* [18] presented new FBG strain sensors with packaging procedures and configurations for strain measurement. Kim *et al* [19] presented a gold-deposited extrinsic Fabry–Perot interferometer for dynamic strain measurement. Yuan *et al* [20] presented a fiber optical 2D strain sensing system for measuring the strain inside a concrete structure. Garcia *et al* [21] developed a novel distributed optical fiber strain sensor suitable for long-distance condition monitoring of engineering structures.

For the application of FBG sensors in tunnels and geotechnical structures, the trend of using FBG sensors is increasingly growing, and some studies concerned have been reported. Li *et al* developed a metal groove encapsulating technique for the bare FBG sensor to measure the surface strain of the second lining of the tunnel [22], and they also developed a differential FBG strain sensor for monitoring the stability of the tunnel in the backfill and operation periods [23]. Kister *et al* [24] reported the use of Bragg grating sensors for strain and temperature monitoring of reinforced concrete foundation piling.

In this work, based on FBG technology, a special type of FBG strain block sensor is developed. The strain block is characterized by three groups of FBG strain rosettes adhered to three adjacent surfaces of the block, and each strain rosette stuck in the adhesive coating in the form of a 0°–45°–90° arrangement, which can be used to acquire a greater amount of strain sensor data to be accurately monitored during tunnel construction.

2. Measurement principle of FBG sensors

FBG sensors, exhibiting better long-term reliability for being noncorrosive, immune to electromagnetic interference, waterproof and intrinsically safe, have a number of advantages over traditional electrical sensors. As a type of grating sensor, a desired refractive index can be produced through a controlled etching. Accordingly, when each grating is illuminated by a broadband spectrum light source, it acted as a filter reflecting a narrowband spectrum of the incident light and transmitting the remaining signal. The center of the reflected spectrum band can be expressed as [7]

$$\lambda_B = 2n_{\text{eff}}\Lambda, \quad (1)$$

where λ_B is the Bragg central wavelength, n_{eff} is the effective refractive index of the optical fiber core and Λ is the grating period (pitch length).

The effective refraction index is acquired with a FBG sensor by detecting the Bragg wavelength change. This Bragg central wavelength shift alters linearly with some other external perturbations such as temperature and strain. The relationship between the central wavelength, temperature and strain can be expressed as

$$\varepsilon = K_\varepsilon[(\lambda - \lambda_0) - K_b(\lambda_T - \lambda_{T0})], \quad (2)$$

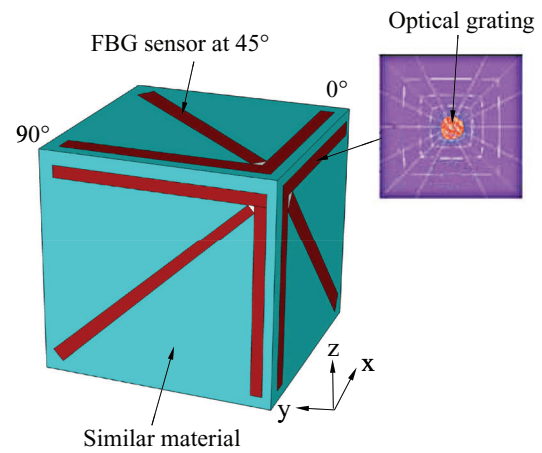


Figure 1. Model of FBG strain sensor.

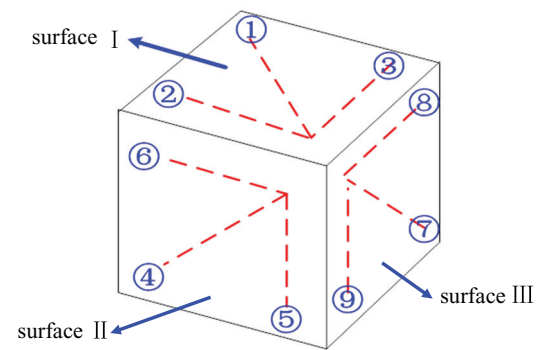


Figure 2. Layout of three groups of strain rosettes.

where K_ε is the strain coefficient; λ is the real-time wavelength, λ_0 is the initial value of wavelength; λ_T is the real-time wavelength with respect to temperature sensor, λ_{T0} is the initial value of wavelength with respect to temperature sensor and K_b is the temperature compensation coefficient.

The grating strain data can be obtained if the offset values of the central wavelength, $\Delta\lambda$ and $\Delta\lambda_T$, are provided.

3. A special type of strain block FBG sensor

3.1. Details regarding the strain block sensor

In order to enhance the reliability of sensors and ensure that strain sensor data is more accurately acquired during tunnel excavation, a special type of FBG strain block sensor for monitoring is introduced, which was developed by Shandong University in China [25, 26]. Three groups of FBG strain rosettes are adhered on three adjacent surfaces of one cubic block separately. On each surface there are a set of strain rosettes, and the sensors are bonded in the form of a 0°–45°–90° arrangement, as illustrated in figure 1. The cubic strain block has a geometry size of 30 × 30 × 30 mm, which is made of similar material with respect to the objective (rock concerned). For the FBG strain block, to facilitate identifying, the three adjacent surfaces are numbered as surfaces I–III, respectively. Therein, surface I is assigned strain sensors from ① to ③ (corresponding to S01, S02, S03), surface II includes sensors from ④ to ⑥ (corresponding to S04, S05, S06), and

Table 1. Parameters of FBG strain sensor.

	Elastic modulus of optical fiber E_f /GPa	Poisson ratio of optical fiber ρ_f	Radius of optical fiber $r_f/\mu\text{m}$	Elastic modulus of similar material E_b /MPa	Poisson ratio of similar material ρ_b
Value	72	0.17	62.5	259	0.268

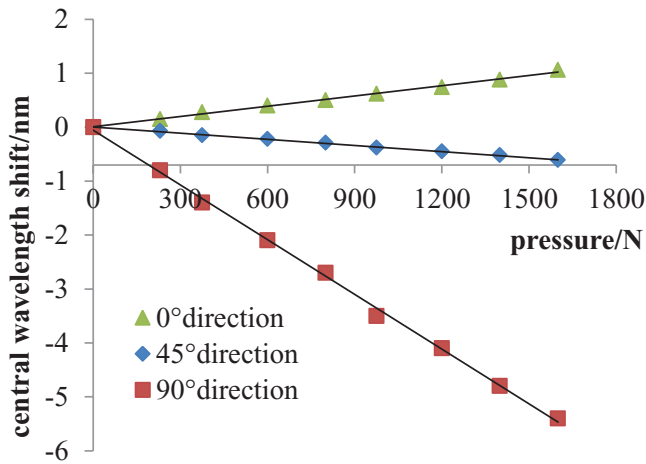


Figure 3. Calibration curves of the FBG strain block.

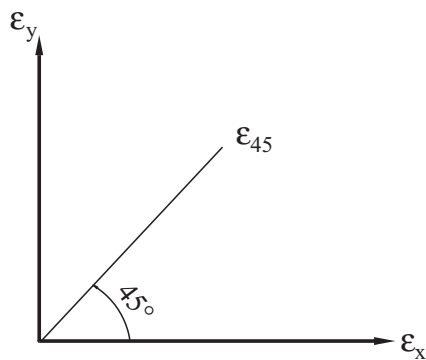


Figure 4. Strain at angle of 45°.

surface III includes sensors from ⑦ to ⑨ (corresponding to S07, S08, S09), as shown in figure 2.

This type of FBG strain sensor only consists of optical fiber, matrix and adhesive coating (the adhesive coating is used for adhesive and packaging protection), so it can avoid complicated transmission such as between metal sleeves and adhesives in some common strain sensors. The detailed fabrication of the strain block can be found in the literature [27]. According to [27], the effect of adhesive with different elastic modulus on the strain response of a block sensor in the directions of 0°, 45° and 90° at one surface was studied by compressive test and numerical modeling, and we concluded that the adhesive with an elastic modulus of 300MPa is the best choice, which is between the elastic modulus of optical fiber and matrix, achieving a good match of fiber and strain block [28]. The parameters of the FBG strain sensor are listed in table 1.

Since it is a type of trifarious FBG sensor block integrating optical fiber, matrix and adhesive coating, the calibration test for the FBG sensor is performed along the directions of 0°, 45° and 90° at each surface. The compressive test for calibration

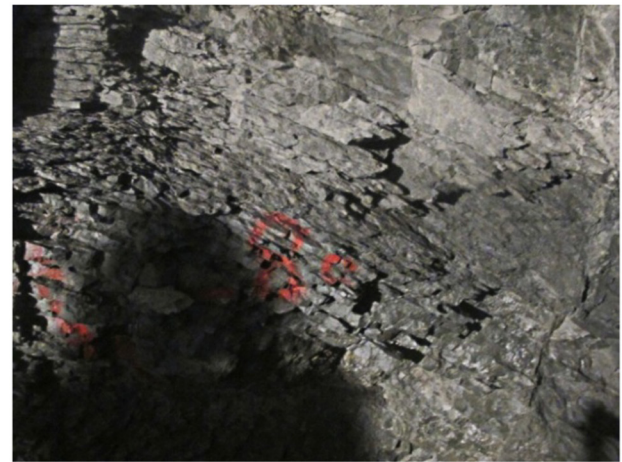


Figure 5. Photo of muddy shale at the sidewall of tunnel.



Figure 6. Excess of clearance limit after installation of the primary lining.

is conducted step by step, and at each step the pressure of 0.22 MPa is applied, for a total of eight steps. Figure 3 presents the typical calibration curves of a strain block along the directions of 0°, 45° and 90°, respectively. These curves are almost straight lines (the correlation coefficients are correspondingly 0.998, 0.994 and 0.998 for 0°, 45° and 90°, respectively), indicating a linear relationship between the central wavelength shift and pressure. Based on calculations, the sensitivity of the strain sensor is $1.09 \text{ pm} \cdot \mu\epsilon^{-1}$, and the transfer coefficient is 0.91, which means that it can be used for strain measurements in engineering applications.

To guarantee the reliability of these strain blocks with FBG sensors, the strain blocks are waterproofed with glue and encapsulated as an integral. After calibration, these strain blocks were tested several times in the laboratory and proved to perform well.

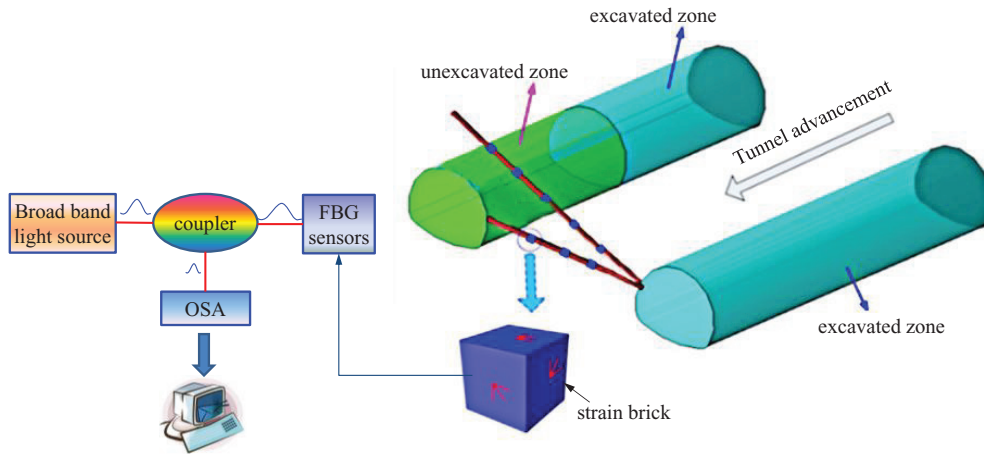


Figure 7. Scheme of monitoring.

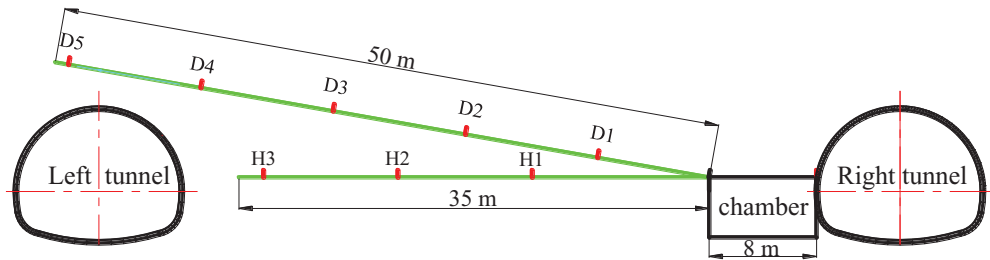


Figure 8. Schematic diagram of drilling and layout of strain blocks.

3.2. Processing method for FBG strain block data

As mentioned above, we can obtain three groups of strain data derived from three surfaces of strain blocks using FBG sensing monitoring. Assuming that one strain block used for measurement is representative of an element located in rock, at one surface of a strain block, a certain strain ε_a with degree α can be derived via

$$\varepsilon_a = \varepsilon'_x \cos^2 \alpha + \varepsilon'_y \sin^2 \alpha + \gamma'_{xy} \sin \alpha \cos \alpha, \quad (3)$$

where ε'_x is the X axial strain, ε'_y is the Y axial strain and γ'_{xy} is the shear strain at X-Y plane.

When α equals 45° , the strain ε_{45} (as shown in figure 4) can be written as

$$\varepsilon_{45} = \varepsilon'_x \cos^2 45 + \varepsilon'_y \sin^2 45 + \gamma'_{xy} \sin 45 \cos 45 = \frac{1}{2} (\varepsilon'_x + \varepsilon'_y + \gamma'_{xy}). \quad (4)$$

In formula (4), ε'_x , ε_{45} and ε'_y can be monitored and converted at one surface by *in situ* FBG sensors, hence the shear strain γ'_{xy} can be derived via formula (4):

$$\gamma'_{xy} = 2\varepsilon_{45} - \varepsilon'_x - \varepsilon'_y. \quad (5)$$

As a result, ε'_x , ε'_y and γ'_{xy} at one surface can be obtained. In the same manner, strains of another two surfaces (planes x-z and y-z) of a strain block can be obtained, which are ε'_x , ε'_z , γ'_{xz} and ε'_y , ε'_z , γ'_{yz} , respectively. By averaging each strain component in the same direction, six strain components of an element, which are ε_x , ε_y , ε_z , γ_{xy} , γ_{xz} , γ_{yz} , can be obtained.

Since six strain components of an element (may be regarded as a point in rock) can be obtained by testing strain block sensors, the strain state of a point and even the whole body in the

ground can be understood (if enough strain block sensors are mounted), which are helpful in analyzing the ground stability in underground engineering.

4. Application in a deep-buried tunnel in squeezing rock

4.1. Background of the tunnel

A deep-buried tunnel, the Xiakou tunnel, was chosen to carry out a test of an engineering application with this type of FBG strain block sensor. The Xiakou tunnel, as a part of Yi-Ba highway, is located in Xingshan city in Hubei province, China. The tunnel is a four-lane, two-way separated tunnel, the left tube of which ranges from chainage ZK104 + 214 to ZK110 + 670, with a length of 6456 m, and the right tube of which is from chainage YK104 + 223 to YK110 + 710, whose length is 6487 m. Besides, the maximum buried depth is about 1500 m, so it is considered to be a super long deep-buried tunnel [29].

According to an *in situ* test, the maximum principle stress is up to 35.14 MPa, primarily characterized by tectonism, which means the tunnel is situated at a very high geostress area. In addition, the lithologies are primarily black shale and muddy shale (figure 5), which belong to soft fractured rocks. Shortly after tunnel excavation, large squeezing deformation arose at the whole cross section. Through field measurements, the crown settlement and deformation at the sidewall amounted to 25 cm and 40 cm, respectively (figure 6), which resulted in exceeding the clearance limit of construction.



(a) Bonding strain blocks on wood sticks



(b) Putting wood sticks into boreholes

Figure 9. Installation of strain blocks.

Due to the large deformation induced, the construction work had to be terminated, and a new scheme for the tunnel excavation and support was required. Considering the geological characteristics of squeezing rock, it often deforms continuously and sustainably. Therefore, to understand the stress or displacement state of surrounding rock to ensure the stability of tunnel construction, a field test based on FBG strain block sensors was conducted.

4.2. Monitoring arrangement

For separated tunnels, to alleviate the mutual disturbance induced by excavation blasting as much as possible, a lagged distance from the excavation face of one tube to that of the other tube is always kept during tunnel construction. In this work, before the large deformation was induced at the left tube, the right tube has headed around 300 m. Accordingly, the right tube can provide room for drilling boreholes from the right tube (excavated section) to the left tube (unexcavated section), as shown in figure 7, so as to conduct a test to monitor strain in the squeezing rock surrounding the left tube.

At the chainage YK106 + 730, due to an existing chamber located at the left side of the right tube, some steps for

Table 2. Parameters of the strain sensors.

Number	Parameters		
	Initial central wavelength λ_0 /nm	Strain coefficient K_ϵ	Temperature compensation coefficient K_b
Sn01	1528	839.038	1.5
Sn02	1533	836.302	1.5
Sn03	1536	834.668	1.5
Sn04	1540	832.501	1.5
Sn05	1544	830.344	1.5
Sn06	1549	827.663	1.5
Sn07	1553	825.532	1.5
Sn08	1558	822.882	1.5
Sn09	1563	820.250	1.5

convenience can be taken. Two boreholes with 110 mm diameter were drilled from the sidewall of the chamber and toward the left tunnel. One borehole is drilled horizontally and its length is 35 m, where three strain blocks were mounted at an average spacing of 10 m, which are numbered as H1, H2 and H3 in order from the chamber. The other borehole was drilled upward at an angle of 10° with respect to the horizontal plane, of which the length is 50 m. Along this borehole five strain blocks were mounted at the same spacing of 10 m, numbered D1, D2, D3, D4 and D5 in order moving away from the chamber, as shown in figure 8.

4.3. In situ installation test

The strain blocks with FBG sensors are well prepared before *in situ* installation. In order to place these strain blocks in the designated positions in the boreholes, wood sticks are employed to place and bond the strain blocks. These wood sticks were selected with a size of 40×15 mm at the cross section, and along the stick direction the designated locations are marked to ensure that the wood sticks are accurately positioned. To prevent the wood sticks from being injured or damaged in the process of advancement, two little sticks are fastened in the front of and behind the strain block (figure 9(a)). Relative to the large deformation induced in squeezing rock, the influence of wood sticks is negligible. After the installation is completed, the two boreholes are backfilled with cement to ensure that the strain blocks with FBG sensors are embedded into the squeezing rock, as shown in figure 9(b). When the strain monitoring system works, data from the FBG sensors in the strain block can be coupled by a coupler in combination with a broadband light source and then transferred to the optical spectrum analyzer (OSA), which is used to detect and output the central wavelength shift. After that, the information about central wavelength shift is submitted to computer. The whole transmission process is illustrated in figure 7.

During the installation of the strain blocks, the FBG temperature sensors were mounted in rock together to ensure temperature compensation. Through monitoring a temperature shift in squeezing rock where the strain blocks are located, strain variation in rock induced by temperature shift

Table 3. Strain ($\mu\epsilon$) in block D5 at chainage YK106 + 730.

Date	Strain block								
	S01	S02	S03	S04	S05	S06	S07	S08	S09
2012-7-25	121.52	35.27	248.44	-166.72	-287.10	25.17	227.19	268.68	-276.64
2012-7-29	125.54	36.42	256.43	-168.51	-290.69	26.32	230.19	276.67	-280.23
2012-7-30	128.35	41.72	258.63	-173.28	-294.76	31.62	215.58	278.87	-284.30
2012-8-22	136.12	44.58	276.21	-178.16	-297.55	34.48	236.66	296.45	-287.09
2012-9-5	148.19	46.39	302.22	-186.32	-307.57	36.29	260.59	322.46	-297.11
2012-9-6	150.94	45.47	308.53	-191.30	-316.57	35.37	261.15	328.77	-306.11
2012-9-7	147.41	46.28	303.10	-194.96	-319.61	36.18	259.24	323.34	-309.15
2012-10-31	196.81	83.69	385.30	-236.95	-390.91	73.59	298.32	405.54	-380.45
2013-1-18	204.69	97.40	403.43	-260.60	-421.55	87.30	300.25	423.67	-411.09

Table 4. Strain ($\mu\epsilon$) components of block D5 at chainage YK106 + 730.

Date	Strain component					
	ϵ_{xx}	ϵ_{yy}	ϵ_{zz}	γ_{xy}	γ_{yz}	γ_{zx}
2012-7-25	258.55	30.23	-281.88	-40.67	-71.51	462.33
2012-7-29	266.54	31.38	-285.47	-41.78	-72.65	463.94
2012-7-30	268.74	36.68	-289.54	-43.65	-83.41	436.58
2012-8-22	286.32	39.54	-292.33	-48.55	-93.25	463.95
2012-9-5	312.33	41.35	-302.35	-52.24	-101.35	495.82
2012-9-6	318.64	40.43	-311.35	-52.12	-101.39	499.64
2012-9-7	313.21	41.24	-314.39	-54.56	-106.48	504.29
2012-10-31	395.41	78.65	-385.69	-75.38	-156.57	571.54
2013-1-18	413.54	92.36	-416.33	-91.45	-186.95	587.92

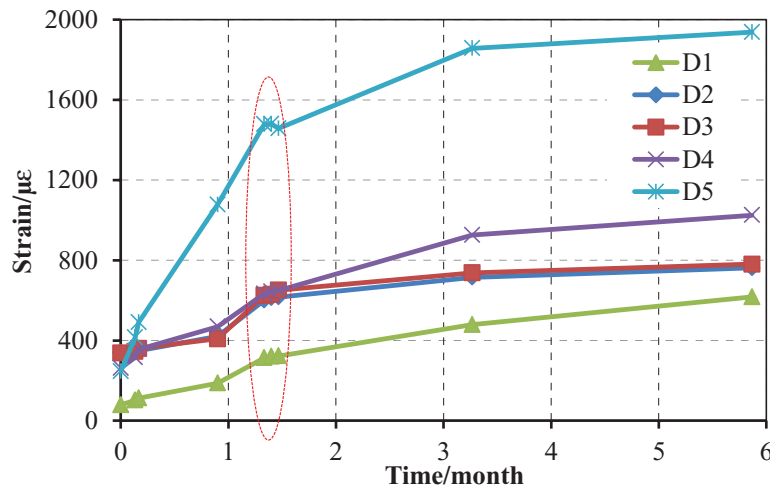


Figure 10. Variation of the first principle strain for strain blocks D1–D5.

can be obtained. Therefore, once the parameters including initial central wavelength λ_0 , strain coefficient K_ϵ and temperature compensation coefficient K_b are presented, block strains in squeezing rock can be derived. The parameters with respect to different strain sensors are listed in table 2.

4.4. Monitoring results

After *in situ* installation, the monitoring test continued for almost half a year. During this period, the right tunnel face approached

and passed through the monitoring section of chainage YK106 + 730. As mentioned above, the main purpose of this test is to monitor and evaluate the strain variation of squeezing rock during and after the excavation at chainage YK106 + 730, which can provide significant information in analyzing the stability of surrounding rock and support when tunneling.

When conducting tests, the data of wavelength shift and wavelength shift with respect to temperature sensor can be acquired and converted to strain via formula (2) automatically using a computer. Table 3 lists strain data of block D5 for nine

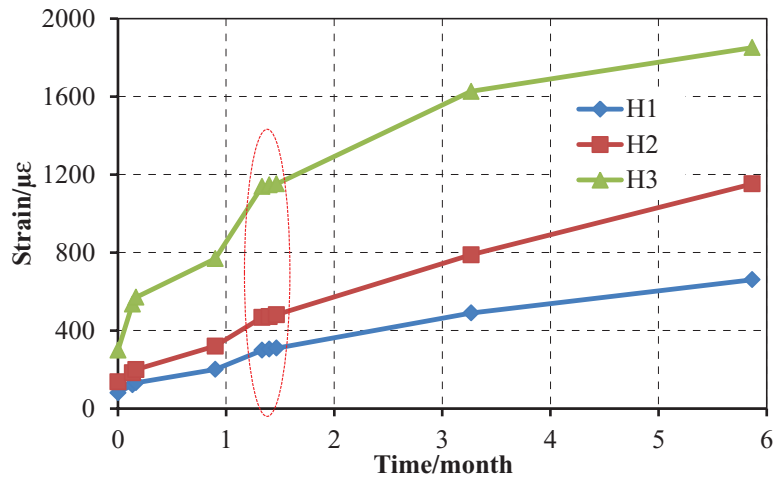


Figure 11. Variation of the first principle strain for strain blocks H1-H3.

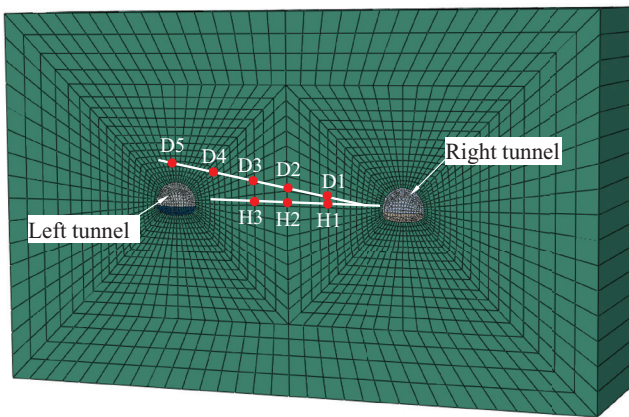


Figure 12. Numerical model.

FBG sensors in a strain block. Using the processing method for the FBG strain block data mentioned in section 3.2, six strain components in a strain block can be transformed. Table 4 lists six strain components of block D5.

Since six strain components monitored in one strain block are representative of those in squeezing rock, strain states at these points in rock can be described. In order to better describe the strain changes in squeezing rock, figures 10 and 11 present the variations of the first principle strain with time for strain blocks D1-D5 and H1-H3, respectively, during the whole monitoring process. Due to the influence of tunnel excavation, abrupt changes of strain in rock can be observed during the period of 5-7 September 2012 (marked with red ellipses). After that, the strains in the rock continue for the effect of rock creep, yet they increase relatively slowly. Compared to strains monitored in the upward borehole (i.e. D1-D5), strains in the horizontal borehole (i.e. H1-H3) have experienced more rapid changes in rock. That is, strain ratios in the blocks for H1-H3 are larger than those of blocks D1-D5, which results from the predominant effect of the horizontal tectonic stress when tunneling. These monitoring achievements can be used to analyze the stability and parameter optimization of surrounding rock and support so as to achieve the desired purpose.

Table 5. Computational parameters of the squeezing rock.

Elasticity modulus/GPa	Poisson's ratio ν	Cohesion C /MPa	Internal friction angle φ (°)
0.80	0.31	0.70	37

Table 6. Comparison of strain results from monitoring and calculation.

Testing point	Monitoring	Calculation	Relative difference (%)
D1	313.29	394.91	26.05
D2	600.19	691.09	15.15
D3	624.44	746.76	19.59
D4	633.28	651.32	2.85
D5	1478.12	1575.57	6.59
H1	298.58	353.40	18.36
H2	467.38	560.38	19.90
H3	1139.01	1287.52	13.04

4.5. Verification by numerical simulation

To further verify the feasibility of the FBG strain blocks used in measuring strains in squeezing rock, a numerical simulation is conducted. A quasi-3D numerical model representative of the chainage YK106 + 730 is established, as shown in figure 12, which considers the locations of these FBG strain blocks. Due to abrupt changes in the strain monitored in rock during tunnel excavation, in this work, we model the excavation of the left tunnel and stress release in the surrounding rock, then focus on changes in displacement and strain in the surrounding rock. The whole simulation can be described in two steps: the first step is stress equilibration of the model under the condition of being excavated for the right tunnel; the second is the excavation of the left tunnel.

In the design stage of the Xiakou tunnel, the preliminary mechanical parameters of the squeezing rock were selected according to some geological exploration achievements [30], as shown in table 5. After simulation, the strain results in the rock where these FBG blocks are positioned can be extracted from the strain field. Table 6 summarizes the comparison of

the strain results in these strain blocks from monitoring and calculation. It can be seen that the results from calculation are comprehensively larger than those from monitoring, some even exceed by 20%, which is the reason that FBG strain blocks failed to monitor some part of the strain in the rock at the initial stage, whereas the simulation calculation can include this part of the strain for its modelling. Nevertheless, the calculation analysis can help support the rationality of the strain results in these strain blocks. So the FBG strain blocks can be applicable in measuring strains in squeezing rock.

5. Conclusions

In order to acquire strain sensor data to be accurately monitored during tunnel excavation, a special type of strain cubic block with FBG sensors has been introduced. The strain block is characterized by three groups of FBG strain rosettes glued on three adjacent surfaces of the block respectively, and each strain rosette distributed in the form of a 0°–45°–90° arrangement. Through the processing method of the FBG strain block, the original strain data of three surfaces of a strain block can be transformed to six strain components, which is regarded as an element of representing the strain state of a point in rock mass.

Applying this type of strain block sensor to a deep-buried tunnel in squeezing rock, optical fiber data at three surfaces of a strain block was acquired, and then the six strain components of each strain block were derived using the processing method for FBG strain block data. The monitoring results can reflect the effect of tunnel excavation due to the abrupt changes in strain monitored in rock during excavation, and were verified to be in good agreement with our numerical simulation. Therefore, FBG strain blocks can be applicable in measuring strains in squeezing rock.

Acknowledgments

This work was financially supported by the National Natural Science Foundation of China (Grant No. 51379007) and the support of the Chinese Fundamental Research (973) Program through Grant No. 2013CB036006. The authors also wish to thank Professors Shucaï Li, Qingmei Sui and Jing Wang of Shandong University for their help with some of the details of the experiment.

ORCID iDs

Guojun Wu  <https://orcid.org/0000-0003-4097-1752>

References

- [1] Aydan Ö, Akagi T and Kawamoto T 1993 The squeezing potential of rocks around tunnels; theory and prediction *Rock Mech. Rock Eng.* **26** 137–63
- [2] Feng X T and Hudson J A 2010 Specifying the information required for rock mechanics modelling and rock engineering design *Int. J. Rock Mech. Min.* **47** 179–94
- [3] Marinos P and Hoek E 2001 Estimating the geotechnical properties of heterogeneous rock masses such as flysch *Bull. Eng. Geol. Environ.* **60** 85–92
- [4] Dai F, Park M W, Sandidge M and Brilakis I 2015 A vision-based method for on-road truck height measurement in proactive prevention of collision with overpasses and tunnels *Autom. Constr.* **50** 29–39
- [5] Dias D and Kastner R 2013 Movements caused by the excavation of tunnels using face pressurized shields—Analysis of monitoring and numerical modeling results *Eng. Geol.* **152** 17–25
- [6] Lai J, Qiu J, Chen J, Fan H and Wang K 2015 New technology and experimental study on snow-melting heated pavement system in tunnel portal *Adv. Mater. Sci. Eng.* **2015** 1–11
- [7] Ye X, Ni Y and Yin J 2013 Safety monitoring of railway tunnel construction using FBG sensing technology *Adv. Struct. Eng.* **16** 1401–9
- [8] Zhao Y, Li Z Q and Dong Y 2014 Design and experiments on a wide range fiber Bragg grating sensor for health monitoring of coal mines *Optik* **125** 6287–90
- [9] Gill A, Peters K and Studer M 2004 Genetic algorithm for the reconstruction of Bragg grating sensor strain profiles *Meas. Sci. Technol.* **15** 1877–84
- [10] Ma Y C, Yang Y H, Li J M, Yang M W, Tang J and Liang T 2012 Dynamic and static strain gauge using superimposed fiber Bragg gratings *Meas. Sci. Technol.* **23** 105202
- [11] Schizas C, Stutz S, Botsis J and Coric D 2012 Monitoring of non-homogeneous strains in composites with embedded wavelength multiplexed fiber Bragg gratings: a methodological study *Compos. Struct.* **94** 987–94
- [12] Feng X, Zhang X, Sun C, Motamedi M and Ansari F 2014 Stationary wavelet transform method for distributed detection of damage by fiber-optic sensors *J. Eng. Mech.* **140** 1–11
- [13] Peters K, Studer M, Botsis J, Iocco A, Limberger H and Salathé R 2001 Embedded optical fiber Bragg grating sensor in a nonuniform strain field: measurements and simulations *Exp. Mech.* **41** 19–28
- [14] Rodriguezcobo L, Marques A T and Santos J L 2013 New design for temperature-strain discrimination using fiber Bragg gratings embedded in laminated composites *Smart Mater. Struct.* **22** 105011
- [15] Zhou G, Sim L M and Loughlan J 2004 Damage evaluation of smart composite beams using embedded extrinsic Fabry–Perot interferometric strain sensors: bending stiffness assessment *Smart Mater. Struct.* **13** 1291–302
- [16] Liu T, Wu M, Rao Y, Jackson D A and Fernando G F 1998 A multiplexed optical fibre-based extrinsic Fabry–Perot sensor system for *in situ* strain monitoring in composites *Smart Mater. Struct.* **7** 550–6
- [17] Gangopadhyay T K, Majumder M, Chakraborty A K, Dikshit A K and Bhattacharya D K 2009 Fibre Bragg grating strain sensor and study of its packaging material for use in critical analysis on steel structure *Sens. Actuators A* **150** 78–86
- [18] Torres B, Payá-Zaforteza I, Calderón P A and Adam J M 2011 Analysis of the strain transfer in a new FBG sensor for structural health monitoring *Eng. Struct.* **33** 539–48
- [19] Kim D H, Park J W, Kang H K, Hong C S and Kim C G 2002 Measuring dynamic strain of structures using a gold-deposited extrinsic Fabry–Perot interferometer *Smart Mater. Struct.* **12** 1–5
- [20] Yuan L, Li Q, Liang Y, Yang J and Liu Z 2001 Fiber optic 2D sensor for measuring the strain inside the concrete specimen *Sens. Actuators A* **94** 25–31
- [21] Garcia M J, Ortega J A, Chavez J A and Salazar J 2002 A novel distributed fiber-optic strain sensor *IEEE Trans. Instrum. Meas.* **51** 685–90

- [22] Li C, Zhao Y G, Liu H, Wan Z, Zhang C and Rong N 2008 Monitoring second lining of tunnel with mounted fiber Bragg grating strain sensors *Autom. Constr.* **17** 641–4
- [23] Li C, Zhao Y G, Liu H, Wan Z, Xu J C, Xu X P and Chen Y 2009 Strain and back cavity of tunnel engineering surveyed by FBG strain sensors and geological radar *J. Intell. Mater. Syst. Struct.* **20** 2285–9
- [24] Kister G, Winter D, Gebremichael Y M, Leighton J, Badcock R A, Tester P D, Krishnamurthy S, Boyle W J O, Grattan K T V and Fernando G F 2007 Methodology and integrity monitoring of foundation concrete piles using Bragg grating optical fibre sensors *Eng. Struct.* **29** 2048–55
- [25] Wang Z F, Wang J, Sui Q M, Liang X M, Jia L, Li S C and Lu S D 2015 Development and application of smart geogrid embedded with fiber Bragg grating sensors *J. Sensors* **2015** 108209
- [26] Jiang S C, Wang J, Sui Q M, Ye Q L and Wang L J 2015 Study of three-component FBG vibration sensor for simultaneous measurement of vibration, temperature, and verticality *J. Sensors* **2015** 1–9
- [27] Wang J, Li S, Shi B, Sui Q, Wang Z, Jiang S, Jia L and Cao Y 2013 Trifarious FBG sensor strain transfer characteristics and its application to tunnel excavation model test *J. Eng. Geol.* **21** 182–9
- [28] Wang J, Li S, Sui Q, Zhang Q, Chen X, Wang Z, Bai T and Shi B 2012 Study of FBG strain sensors based on similar materiel in zonal disintegration model test *J. China Coal Soc.* **37** 1570–5
- [29] Li H B, Dai Y H, Song J H and Fu K J 2011 Construction monitoring for Xiakou soft rock tunnel under high geostress and its supporting measures *Rock Soil Mech.* **32** 496–501
- [30] Tian H, Chen W, Zheng P and Yu J 2013 Study of section optimization for high geostress soft rock tunnel considering rheological effect *Rock Soil Mech.* **34** 265–71